Energy and Built Environment xxx (xxxx) xxx

Contents lists available at ScienceDirect

Energy and Built Environment

journal homepage: http://www.keaipublishing.com/en/journals/energy-and-built-environment/

Annual performance of solar chimney for a multi-story building based on Modelica multizone model

Yimin Liao, Zhi Gao*, Fusuo Xu

School of Architecture and Urban Planning, Nanjing University, 22 Hankou Road, Nanjing, Jiangsu 210093, China

ARTICLE INFO

Keywords:
Solar chimney
Natural ventilation
Energy performance
Modelica
Multizone airflow networks

ABSTRACT

Integration of solar chimney is an effective passive strategy for facilitating fresh air flow and offering significant potential for building energy conservation. This research evaluates the optimal design and control strategy for a six-story office building that includes a solar chimney, focusing on stack effect ventilation and energy performance throughout the year. The ventilation rates in different configurations of solar chimney are compared to meet fresh air requirements. The results indicate that the separated solar chimney ensures uniform airflow across each floor, with ventilation standard-reaching rates ranging from 79.5 % to 88.6 %. Furthermore, maximums of air flow rate occur at each floor, with critical cavity width values of 0.5 m, 0.4 m, 0.4 m, 0.3 m, 0.3 m, and 0.2 m on the 1st to 6th floor, respectively. Under the condition of equal cavity inlet area, air flow rates rise with the increasing length/width ratios. Finally, when the outdoor temperatures fall beyond the design range, controlling excessive ventilation generated by solar chimney leads to a 19.6 % reduction in total energy consumption over the year, with 71.5 % of the savings during winter.

1. Introduction

Modern buildings typically depend on mechanical ventilation systems to supply fresh air and enhance indoor thermal comfort. However, this reliance often results in significant energy consumption and carbon emissions. Diana et al. [1] provided statistics indicating that heating and cooling constitute a substantial portion of total building energy usage, ranging from 18 % to 73 % globally. In contrast to mechanical ventilation, effective passive strategies of natural ventilation offer promising potential for energy conservation and reduction of greenhouse gas emissions [2–6].

The solar chimney, which utilizes the stack effect to drive airflow, represents a dependable passive ventilation system. Solar radiation penetrates through the glazing and is received by the absorbing plate. The warmed air within the cavity ascends due to buoyancy-driven forces, facilitating the inflow of fresh air into the room through window openings. Lee et al. [7] observed that employing thermal chimneys resulted in savings of 20.4 %, 18.9 %, and 13.1 % in cooling load, respectively, across three cities (Spokane, Phoenix, and Minneapolis, USA) under varying climatic conditions. Miyazaki et al. [8] conducted the computational fluid dynamics (CFD) simulation on solar chimney buildings in Japan, demonstrating a potential reduction of approximately 50 % in fan shaft power requirements and 20 % in heating load during the heating season. The solar chimney is gaining increasing attention from researchers and engineers because of its notable benefits in enhancing natural ventilation, improving thermal comfort, reducing energy consumption, and minimizing operational costs [9–12].

Numerous scholars analyzed the heat transfer process induced by solar radiation and developed mathematical models to predict temperature distribution and airflow rates based on energy balances [13–15]. He et al. [16,17] introduced a plume model incorporating density variations in both horizontal and vertical directions to predict airflow rates and reveal an optimal chimney gap for maximum flow rate. Herrero [18] established one-dimensional unsteady-state mathematical models for air temperature distribution in chimney channels. Subsequent modifications to parameters such as flow coefficient and story correction coefficient [19], as well as consideration of backflow due to pressure loss coefficient and thermal boundary effect, resulted in theoretical calculations in closer agreement with actual conditions. However, the complexity of the actual mechanism and numerous influencing factors make it challenging to rely solely on mathematical models. In experimental research, methods such as real-time operational measurements [20,21] and reduced-scale models [22] are commonly employed to optimize chimney height, cavity width, air inlet height, and inclination angle for enhancing ventilation [23]. Tracer gas, particularly, helps to observe airflow patterns [24]. However, experimental studies usually need high input costs and have stringent research environment constraints.

* Corresponding author.
E-mail address: zhgao@nju.edu.cn (Z. Gao).

https://doi.org/10.1016/j.enbenv.2024.05.002
Received 29 February 2024; Received in revised form 9 May 2024; Accepted 10 May 2024
Available online xxx
2666-1233/Copyright © 2024 Southwest Jiatong University. Publishing services by Elsevier B.V. on behalf of KeAi Communication Co. Ltd. This is an open access article under the CC BY-NC-ND license (http://creativecommons.org/licenses/by-nc-nd/4.0/)

Please cite this article as: Y. Liao, Z. Gao and F. Xu, Annual performance of solar chimney for a multi-story building based on Modelica multizone model, Energy and Built Environment, https://doi.org/10.1016/j.enbenv.2024.05.002

In the numerical simulation of building ventilation, the multizone model offers a couple of advantages compared with the CFD method [25–28], which provides detailed flow field information with high precision. For instance, the multizone model, as a lumped model from a macroscopic perspective, is suitable for long-time dynamic simulations due to its faster calculation speed. This model predicts averaged temperatures, concentrations, and mass flow rates by idealizing systems as collections of finite control volumes, where mass, momentum, and energy transport are described using ordinary differential conservation equations [29]. Currently, the multizone method has wide application in the study of building ventilation [30], indoor air pollution [31], indoor thermal comfort, and energy consumption [32].

The Modelica model, a typical multizone model, is commonly utilized for simulating interaction processes in ventilation, heat storage, and heating systems within buildings. Modelica was developed by the Modelica Association, an international organization to oversee the development and promotion of the Modelica language and associated standards. Modelica is a multi-domain modeling language. This versatility allows for integrated modeling of solar chimney systems where energy interactions with other domains need to be considered, including thermal, fluid, and control systems. Modelica supports the modeling of control systems alongside physical systems. This capability is particularly useful for studying the dynamic behavior and performance optimization of solar chimney systems. In building simulations of thermal, fluid, and control systems, scholars have compared and validated the effectiveness and reliability of Modelica simulations with other software or experiments. Wetter [33] proposed using Modelica model to simulate the multizone wind environment in 2006, comparing it with CONTAM for model verification, with a significant fit observed. Stephan et al. [34] applied Wetter's method to simulate indoor natural ventilation, verifying it using SimSPARK. For thermal simulation, Kuznik et al. [35] built a Modelica model to examine the impact of phase change material walls on the indoor thermal environment. Tomazic et al. [36] simulated the dynamic indoor environment and control system on the Modelica platform, developing thermal models for the simulator. The simulation research on solar chimney employing Modelica is still at an initial stage. Leang et al. [37] established a composite Trombe wall model on Modelica platform and verified the model by comparing simulated and measured heat flux, surface temperatures, and fluid temperatures in a ventilated air layer to further explore the effect of new heat storage materials. Gloriant et al. [38] developed a supply-air window model on Modelica platform based on analytical solutions of air circulation between isothermal panes. The supply-air window model, resembling a double-layered glass model, preheats fresh air entering the room through long-wave and short-wave radiation, and convective heat transfer between glass, environment, and air. Validation was achieved through comparison with CFD, and the thermal performance of the supply-air window was studied.

Although many previous studies have identified factors influencing the performance of solar chimneys in buildings, few have specifically addressed the annual dynamic performance of solar chimneys in multi-story buildings. Consequently, this study discusses the optimal design and control strategy of a six-story solar chimney office building based on ventilation performance and thermal comfort throughout the year and ultimately assesses its annual energy-saving efficiency. The simulations in this research are conducted using the Modelica language with the *Buildings* and *BuildingSystems* libraries on the OpenModelica platform.

The structure of this paper is as follows: Section 2 provides an introduction to outdoor meteorological parameters, building model parameters, the approach of numerical simulation in Modelica, the Modelica model, and validation compared with an experiment. Section 3 analyzes the impact of the solar chimney configuration, geometric parameters, and control strategy on ventilation, thermal comfort, and energy efficiency performance. Finally, Section 4 presents the conclusions drawn from this study.

2. Methods

2.1. Meteorological parameters and building parameters

The research site for this study is Nanjing, China, a typical city in hot summer and cold winter areas. As shown in Fig. 1(a), meteorological parameters are sourced from the weather database of the typical meteorological year on the EnergyPlus website. The annual dry bulb temperature ranges from −5.4 °C to 37.2 °C, and the global horizontal radiation ranges from 0 W•h/m^2 to 953 W•h/m^2. The average meteorological data of 15 consecutive days for each season as the representative meteorological parameters are depicted in Fig. 1(b). During summer, stack effect ventilation is primarily driven by solar radiation, whereas in winter, it predominantly arises from the temperature difference between the interior and exterior of the chimney cavity. Analysis of wind speed data reveals that during the daytime period (8:00 - 18:00), calm wind conditions persist for 550 h, representing 13.1 % of the total time, and weak winds, defined as those not exceeding 2 m/s, occur for 1768 h, accounting for 44.0 % of the total duration. Additionally, the wind speed is weakened by the shielding effect of surrounding buildings. Therefore, the ambient environment is characterized by calm wind conditions, and the focus remains primarily on the ventilation performance resulting from air volumes.

A representative six-story office building, oriented southward, was modeled for this case study. Each floor has identical dimensions of 6.0 m × 5.0 m × 3.0 m and features a square openable window measuring 1 m × 1 m located at the center of the north wall. A solar chimney, constructed with 4 mm thick single glazing of plain glass, is attached to the south side, with its air inlet positioned at the bottom of the south wall on each floor. Details regarding the specific structure and geometric dimensions of the solar chimney are provided in Section 2.2. Each office accommodates six human occupants from 8:00 to 18:00, regardless of weekdays, weekends, or holidays, with equipment and lighting in operation. Consequently, the ventilation effect of the solar chimney at night is disregarded. Considering the minimum fresh air requirement of 30 m^3/h per person, the minimum air flow rate is set at 0.05 m^3/s. The total heating loads, encompassing occupants, equipment, and lighting, amount to 25 W/m^2. Split air conditioners are employed to regulate indoor air temperature, maintaining it within the range of 18–28 °C during working hours, under the design standards of comfort air conditioning.

2.2. Numerical approach of Modelica

2.2.1. Equivalent air temperature

Meteorological parameters comprise atmospheric pressure, dry bulb temperature, relative humidity, wind direction, wind speed, etc. The transfer of heat and moisture into the room through the envelope structure and air infiltration significantly impacts the indoor thermal and humid environment. This study focuses on the influence of sensible heat on the indoor thermal environment and disregards the effect of latent heat and moisture. For exterior walls and glazing cover, solar radiation received on their outer surface includes direct radiation, sky diffuse radiation, and ground reflection. Hence, the equivalent air temperature of the outer surface comprehensively accounts for the effect of solar radiation. The equivalent air temperature on the exterior wall can be calculated as follows, incorporating a correction term:

$$T_{EqAirExt} = T_{AirAmb} + \Delta T_{EqLW} + \Delta T_{EqSW} \quad (1)$$

where $T_{EqAirExt}$ (K) is the equivalent air temperature on the outer surface of the exterior wall for computing the heat transfer between the exterior wall and the indoor environment. T_{AirAmb} (K) is the ambient air temperature. ΔT_{EqLW} (K) and ΔT_{EqSW} (K) are the corrected long-wave and short-wave radiation temperatures, respectively. The correction of long-wave radiation is determined by the blackbody sky temperature and dry bulb temperature, and the correction of short-wave radiation

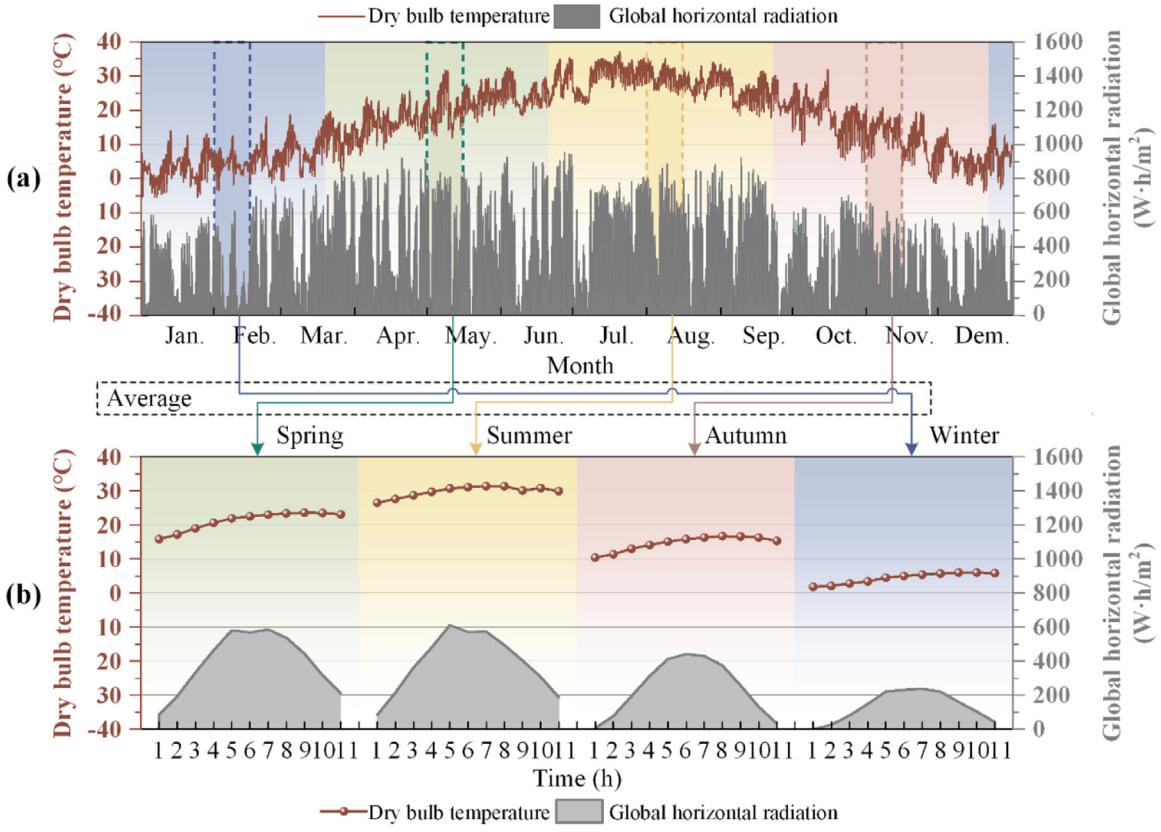


Fig. 1. Meteorological parameters. (a) All year round, (b) Typical seasonal day.

depends on the solar radiation in a specific direction, which can be calculated by:

$$\Delta T_{EqLW} = \frac{(T_{BlaSky} - T_{DryBul})h_{Rad}}{h_{Rad} + h_{WExt}} \tag{2}$$

$$\Delta T_{EqSW} = \frac{H_{Sol}\mathrm{a}_{Ext}}{h_{Rad} + h_{WExt}} \tag{3}$$

Where T_{BlaSky} (K) is the blackbody sky temperature. T_{DryBul} (K) is the dry bulb temperature. h_{Rad} (W/(m^2•K)) is the radiative heat transfer coefficient. h_{WExt} (W/(m^2•K)) is the convective heat transfer coefficient of the external façade. H_{Sol} (W/m^2) is solar radiation intensity. a_{Ext} is absorptance.

The correction of short-wave radiation is not incorporated in the calculation of the equivalent air temperature of glazing. Instead, it is addressed in subsequent steps.

2.2.2. Heat transfer of the glazing

Solar radiation penetrates the transparent glazing cover, significantly influencing the thermal environment within the chimney cavity, often exerting a more substantial impact than heat conduction. Sensible heat transfer into the cavity through the glazing cover has two components: heat transfer ($Q_{GlaTrans}$) and solar radiation heat gain (Q_{GlaSol}). Due to the weak coupling relationship between the two components, they are solved independently. Because of its minimal heat capacity, the thermal inertia of the glazing is typically neglected, and the heat transfer is approximately as steady-state. The heat transfer through glazing is given by:

$$Q_{GlaTrans} = U_{Gla}A_{Gla}\left(T_{EqAirGla} - T_{Cav}\right) \tag{4}$$

where U_{Gla} (W/(m^2•K)) denotes the heat transfer coefficient of the glazing. A_{Gla} (m^2) is the area of the glazing corresponding to the single layer. $T_{EqAirGla}$ (K) is the equivalent air temperature on the outer surface of the glazing. T_{Cav} (K) is the cavity air temperature.

After solar radiation falls on the glazing cover, a portion of it is reflected off. Another portion transmits directly into the cavity, contributing to the heat gain of chimney cavity. The remainder is absorbed by glazing, elevating its temperature. Some of this absorbed heat is transferred into the cavity through convection and radiation, while the rest dissipates outdoors and does not contribute to the heat gain. The calculation of the heat absorbed by glazing and subsequently introduced into the cavity is considered in the convective heat transfer between the inner surface of the glazing and the air in the cavity. Therefore, the solar radiation heat gain through glazing can be expressed as follows:

$$Q_{GlaSol} = Q_{Gla,\tau} + Q_{Gla,\alpha} \tag{5}$$

where $Q_{Gla,\tau}$ (W) is the solar radiation heat gain transmitted through glazing. $Q_{Gla,\alpha}$ (W) is the heat gain absorbed by glazing and subsequently introduced into the cavity.

$$Q_{Gla,\tau} = q_{Sol}g_{Win}r_{WinConRad}A_{Gla} \tag{6}$$

$$Q_{Gla,\alpha} = q_{Sol}g_{Win}\left(1 - r_{WinConRad}\right)h_{GlaIn}\left(T_{GlaIn} - T_{Cav}\right)A_{Gla} \tag{7}$$

where q_{Sol} (W/m^2) is the solar radiation intensity falling on the exterior surface of the glazing. In OpenModelica simulation, the computation of short-wave radiation through glazing with any orientation and inclination is facilitated by solar transmission correction factors. Furthermore, g_{Win} is the solar heat gain coefficient. h_{GlaIn} (W/(m^2•K)) is the convective heat transfer coefficient of the internal surface of the glazing. T_{GlaIn} (K) is the temperature at the internal surface. $r_{WinConRad}$ is a ratio for glazing between cavity convective and radiative heat transfer:

$$r_{WinConRad} = \frac{\alpha}{1 - \beta} = \frac{\alpha}{\alpha + \tau} \tag{8}$$

where α is the absorptivity of the glazing; β is the reflectivity; τ is the transmissivity.

2.2.3. Stack effect ventilation

The air within the chimney cavity is assumed to be fully mixed. The pressure difference on both sides of the chimney orifices drives the airflow. The equation is:

$$q_v = C_D A \sqrt{\frac{2}{\rho_0}} \Delta p^m \tag{9}$$

where q_v (m^3/s) is the volumetric flow rate. Δp (Pa) is the pressure difference across the orifice, m is the flow exponent of the orifice. C_D is the discharge coefficient of the cavity orifice. A (m^2) is the cross-section area. ρ_0 (kg/m^3) is the mass density at the default standard pressure, temperature, and humidity.

For the airflow exchange between chimney cavities, the variation of pressure in a large volume should be taken into consideration. The air column between points a (at the top) and b (at the bottom) can be viewed as a uniformly mixed vertical shaft with a height of H_{ab} and a mass density of ρ_m, where the absolute pressure decreases and the relative pressure increases with increasing height. The pressure difference Δp_{ab} is given by:

$$\Delta p_{ab} = -H_{ab}\rho_m g = p_a - p_b \tag{10}$$

where H_{ab} (m) is the height of the shaft. ρ_m (kg/m^3) is the mass density of the uniformly mixed vertical shaft. g (m/s^2) is the standard acceleration of gravity. p_a (Pa) and p_b (Pa) are the absolute pressure at points a and b, respectively. The parameter Δp_{ab} remains negative.

2.2.4. Air flow through the window

The air flows bi-directionally through the open north window, which utilizes discretization along the height coordinate. Additionally, an input signal $0 \le y \le 1$, the fraction of aperture that is open, is incorporated to control the opening and closing of the window. The volume flow rate for each discretization compartment is calculated by:

$$Q_{win} = k_{Win} sign(\Delta P_{Win}) |\Delta P_{Win}|^{m_{Win}} \tag{11}$$

$$m_{Win} = y m_{Ope} + (1-y) m_{Clo} \tag{12}$$

$$k_{Win} = y k_{Ope} + (1-y) k_{Clo} \tag{13}$$

$$k_{Ope} = C_{DWin} \frac{A_{Ope}}{n_{Com}} \sqrt{\frac{2}{\rho_0}} \tag{14}$$

$$k_{Clo} = C_{DWin} \frac{A_{Clo}}{n_{Com}} \sqrt{\frac{2}{\rho_0}} \tag{15}$$

$$A_{Ope} = W_{Ope} h_{Ope} \tag{16}$$

$$A_{Clo} = C_{DWin} L_{Clo} \tag{17}$$

where ΔP_{Win} (Pa) is the pressure difference between compartments. m_{Win} is the flow exponent of window. m_{Ope} and m_{Clo} are the flow exponent of open and closed window, respectively. k_{Win} is the flow coefficient of the window. k_{Ope} and k_{Clo} are the open and closed aperture flow coefficient of window, respectively. C_{DWin} is the discharge coefficient of window. A_{Ope} and A_{Clo} are the open and closed aperture areas of window, respectively. n_{Com} is the number of compartments for the discretization. L_{Clo} is the effective leakage area of closed aperture. W_{Ope} is the width of open aperture. h_{Ope} is the height of open aperture. The parameter y can be adjusted to simulate various conditions and can also be altered according to actual situation.

2.2.5. Heating and cooling of the air conditioner

The air conditioning system monitors the indoor temperature in real time and judges whether it falls within the appropriate preset range. If it falls outside this range, the system activates cooling or heating. It's important to note that this study employs an ideal air conditioning model to investigate energy consumption without an additional mechanical fresh air system. The heating and cooling functions of the air conditioner are reflected by positive and negative heat flow.

The control of the output heat flow of the air conditioning system is realized by the PID (Proportional-Integral-Derivative) controller. Despite the emergence of numerous advanced controllers, the PID controller has still been widely adopted in industrial process control due to its exceptional performance in simplifying algorithms, robustness, and stability.

The constants used in the Modelica simulation to describe the geometric dimensions and physical process are shown in Table 1.

2.3. Modelica model

Based on OpenModelica v1.13.264, the Modelica model shown in Fig. 2 presents a single-story building with a solar chimney. Multi-story building models with various structures and configurations will be given in Section 3. Four models (Model 1–4) composed of different modules (Module A-G) are employed to study the effects of solar chimney configuration, geometric parameters, and control strategy on annual ventilation rate and air conditioning energy consumption. Module A, named *Weather*, serves to read, process, transform, and transmit weather data, and calculate equivalent air temperature and comprehensive radiation. Module B, named *Building envelope*, computes the heat transfer across exterior walls, windows, roof, and floor, considering thermal resistance and heat capacity. Module C, named *Window*, applies *DoorDiscretizedOperable* model from the *Modelica* library, which offers options for dynamic-controlled and fixed-setting openings. Module D, named *Air conditioning*, is primarily implemented through the PID controller model, indoor temperature sensor model, and math and logical models. By continuously monitoring and providing feedback on indoor temperature, this module determines the operation mode of the air conditioning system. Module E, named *Stack effect ventilation*, incorporates a completely mixed fluid volume and considers the pressure difference caused by the stack effect. Module F, named *Glazing*, computes the heat transfer of glazing and the solar radiation heat gain into the chimney cavity. Lastly, Module G, named *Orifice controller*, regulates the opening of the chimney inlet based on outdoor temperature, indoor temperature, and air flow rate. The details of several critical models are illustrated in Fig. 3.

For multi-story buildings, vertical solar chimneys are commonly installed on the exterior walls, with designs typically falling into two configurations: combined and separated solar chimneys. The combined solar chimney, extensively researched and implemented, incorporates an entrance on each floor and a single exit at the top floor. In contrast, the separated solar chimney is equipped with both entrance and exit points on every floor. Fig. 4 depicts the schematic diagram and Modelica model of the two configurations of solar chimney analyzed in this study.

2.4. Validation

2.4.1. Solar chimney with single inlet

To validate the numerical Modelica model of solar chimney with a single inlet and outlet on one floor (the separated solar chimney), a full-scale experimental study conducted by Bouchair [39] is used for comparison. The corresponding physical model and the Modelica model are depicted in Fig. 5. A room of 1.7 m × 1.9 m × 2.0 m was constructed within a spacious laboratory measuring 20 m × 10 m × 5 m, ensuring steady-state conditions. Air in the chimney cavity was heated by two parallel walls with variable surface temperatures, one wall fixed in position on the room side, and the other movable.

Table 1
Input parameters of the simulated model.

Structure	Constants	Nomenclature	Value	Unit
Building	Lat	Latitude	32	deg
	Azi	Surface azimuth	South=0, East=90	deg
Room	T_0	Initial indoor temperature	293	K
	T_u	Indoor design temperature upper limit	301	K
	T_l	Indoor design temperature lower limit	291	K
	Q_{In}	Indoor total heating loads include occupants, equipment, and lighting	25	W/m^2
Cavity orifice	C_D	Discharge coefficient of cavity orifice	0.65	–
	m	Flow exponent of cavity orifice	0.65	–
Glazing	g_{Win}	Solar heat gain coefficient	0.9	–
	$r_{WinConRad}$	Ratio between cavity convective and radiative heat transfer	0.09	–
	α_G	Thermal conductivity of the glazing	1.1	W/(m·K)
	h_{GlaExt}	Convective heat transfer coefficient of the glazing external surface	20	W/(m^2·K)
	h_{GlaIn}	Convective heat transfer coefficient of the glazing internal surface	10	W/(m^2·K)
Window	A_{Clo}	Effective leakage area of the closed window	0.002	m^2
	C_{DWin}	Discharge coefficient of the window	0.65	–
	m_{Ope}	Flow exponent of the open window	0.5	–
	m_{Clo}	Flow exponent of the closed window	0.65	–
Wall	d_W	Wall thickness	0.3	m
	T_{W0}	Initial internal surface temperature of wall	293	K
	ρ	Wall density	2300	kg/m^3
	α_W	Thermal conductivity of the wall	1.1	W/(m·K)
	h_{WExt}	Convective heat transfer coefficient of the external wall surface	20	W/(m^2·K)
	h_{WIn}	Convective heat transfer coefficient of the internal wall surface	10	W/(m^2·K)
Air conditioner	Q_{Ac}	Air conditioning heating/cooling capacity	7200	W

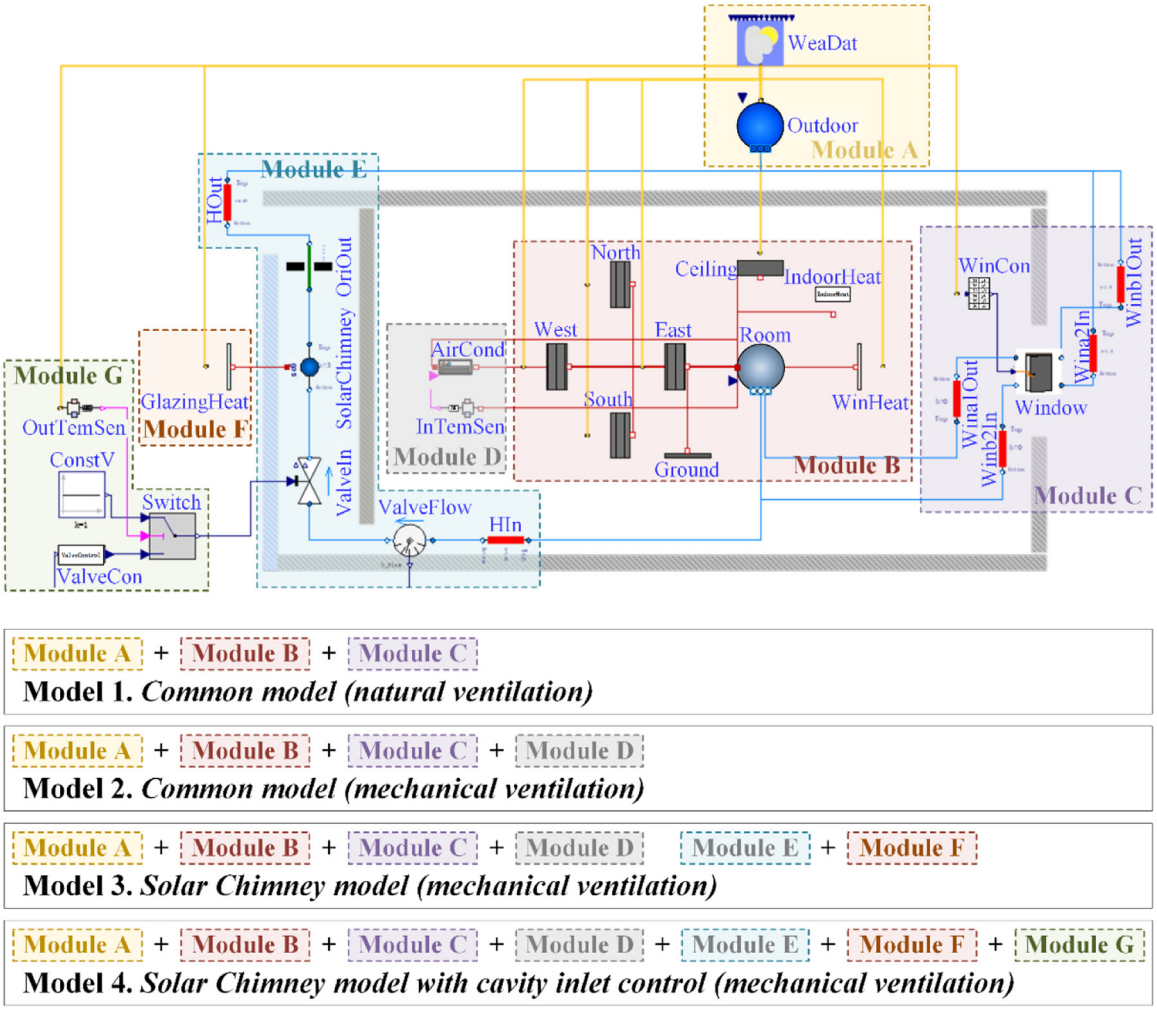


Fig. 2. Modelica model (single-story) of the investigation.

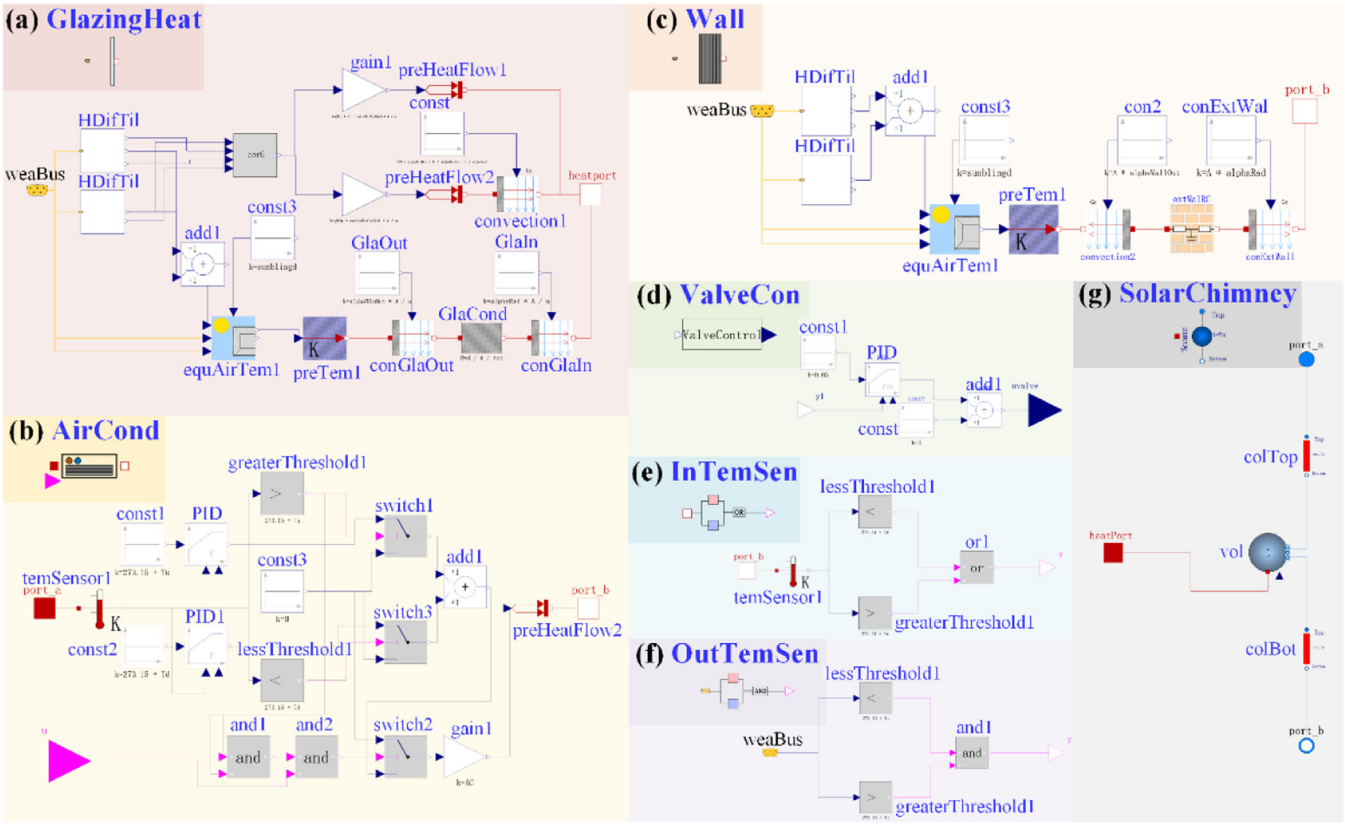


Fig. 3. The details of critical models.

The ambient temperature was maintained at 20 ˚C. Two inner surfaces of the cavity were heated by horizontal electrical heaters to form isothermal surfaces, which output constant heat flow. Except for the heating walls, all other walls were regarded as adiabatic boundaries. To study the ventilation performance of solar chimneys, three parameters were varied as follows:

1) The height of air inlet (0.1 m, 0.4 m)
2) The width of cavity (0.1 m, 0.2 m, 0.3 m)
3) The surface temperature of the heated wall (30 ˚C, 40 ˚C, 50 ˚C, 60 ˚C)

Two standard metrics, normalized mean bias error (NMBE) and coefficient of variation of the root-mean-square error (q_v(RMSE)) [40], were applied to evaluate the accuracy of the numerical simulation. These metrics are defined as follows:

$$NMBE = \frac{\sum_{i=1}^{n}(q_{sim,i} - q_{exp,i})}{n} \times \frac{100\%}{\bar{q}} \tag{18}$$

$$q_v(RMSE) = \sqrt{\frac{\sum_{i=1}^{n}\left(q_{sim,i} - q_{exp,i}\right)^2}{n}} \times \frac{100\%}{\bar{q}} \tag{19}$$

where $q_{sim,i}$ and $q_{exp,i}$ are the simulated and the experimental air flow rates for the i period, n is the number of input values, $\bar{q}$ is the mean of experimental values. The criterion for a credible simulation model is defined by the following statistical metrics: −10 % ≤NMBE≤ 10 %, q_v(RMSE)≤ 30 %.

Fig. 6 illustrates that the simulation results of the Modelica model closely resemble the experimental results, but are slightly smaller. A higher mass flow rate is observed with increasing cavity width or surface temperature. The mean relative error between the Modelica model and the experiment data is 7.0 % for an inlet height of 0.1 m and 8.6 % for an inlet height of 0.4 m. Additionally, all values of NMBE and q_v(RMSE) listed in Table 2 fall within the specified criterion. These results suggest that the Modelica model predicts the airflow rate in good agreement with the experimental results. The errors may be attributed to the following factors:

Table 2
NMBE and q_v(RMSE) values.

Inlet height (m)	Error (%)	Cavity width (m)		
		0.1	0.2	0.3
0.1	q_v(RMSE) (%)	10.74	8.29	4.79
	NMBE (%)	−9.58	−7.90	−4.60
0.4	q_v(RMSE) (%)	11.07	11.17	6.93
	NMBE (%)	−9.58	−7.44	−2.89

1) In the Modelica model, the heat flow into the cavity is calculated by the convective heat transfer coefficients acquired from the experiment. However, it's worth noting that the experiment-calculated coefficient value may be smaller than the actual value.
2) In Fig. 5(b), a *MediumColumn* model named *HIn* is depicted, which computes the pressure difference between the center of the room and the cavity inlet. Usually, the geometric center of the inlet plane is utilized. However, it is remarkable that in the numerical modeling of FDS [41], the temperature near the bottom of the inlet plane is higher, resulting in a larger pressure according to the ideal gas state equation. Consequently, the actual pressure difference is larger than the computed value.

2.4.2. Solar chimney with multiple inlets

Concerning the solar chimney with multiple inlets on a multi-story building (the combined solar chimney), the validation of the numerical Modelica model is confirmed by comparing it with a scale-down experimental study conducted by Gong et al. [42]. As shown in Fig. 7, each

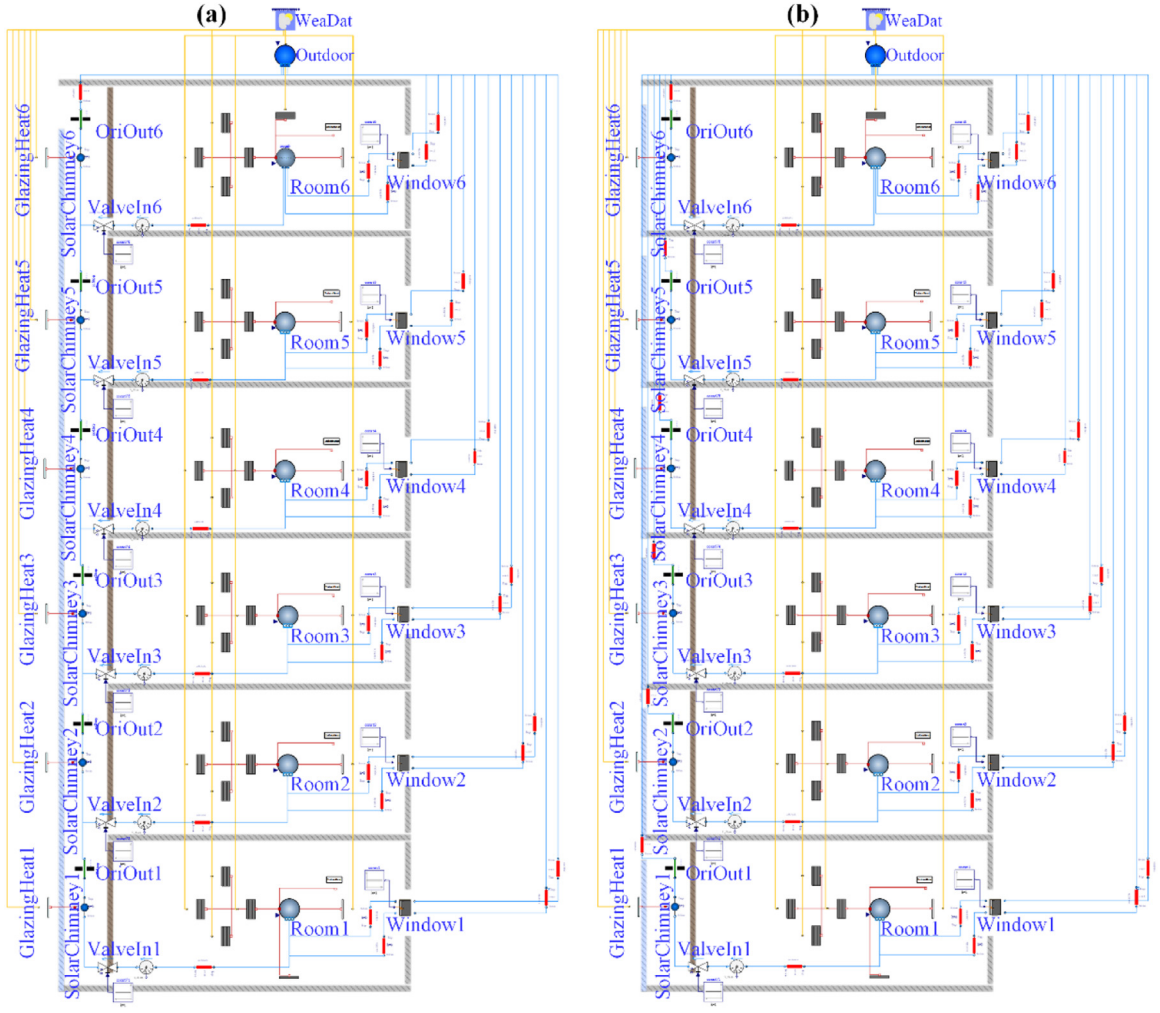


Fig. 4. Modelica model (six-story) of the investigation. (a) The combined solar chimney, (b) The separated solar chimney.

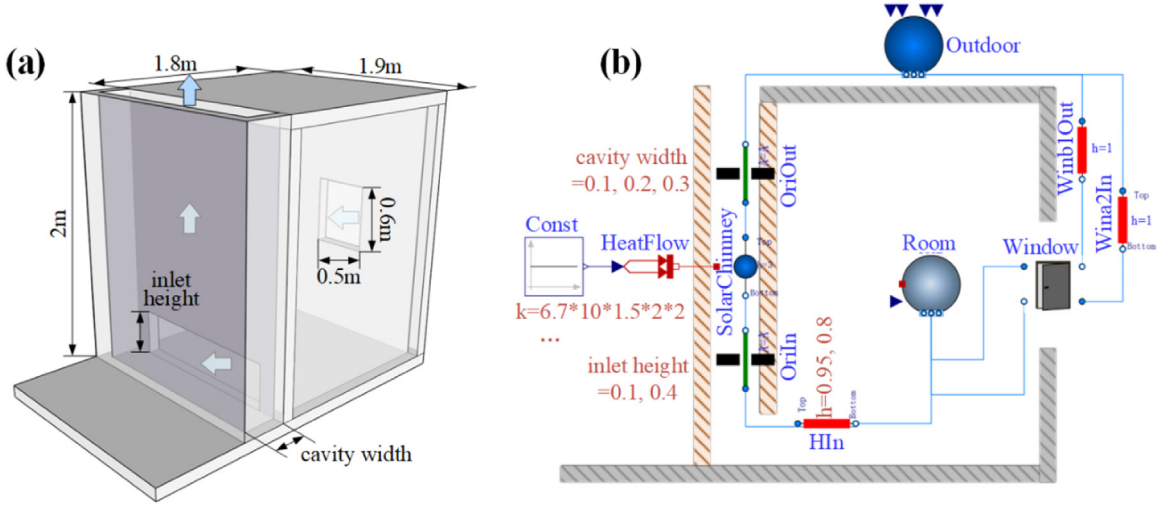


Fig. 5. Validation of the solar chimney with single inlet. (a) Schematic diagram, (b) Modelica model.

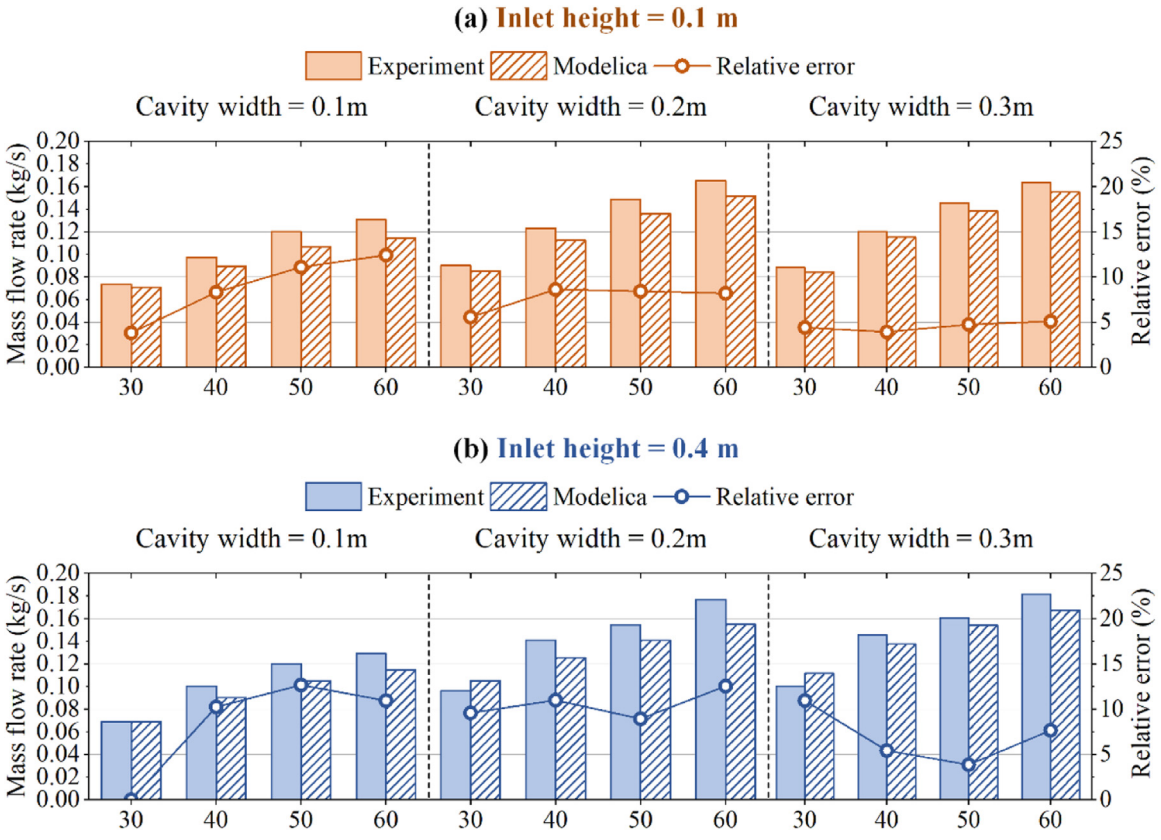


Fig. 6. Validation results. (a) Inlet height =0.1, cavity width=0.1 m, 0.2 m, 0.3 m, (b) Inlet height =0.4, cavity width=0.1 m, 0.2 m, 0.3 m.

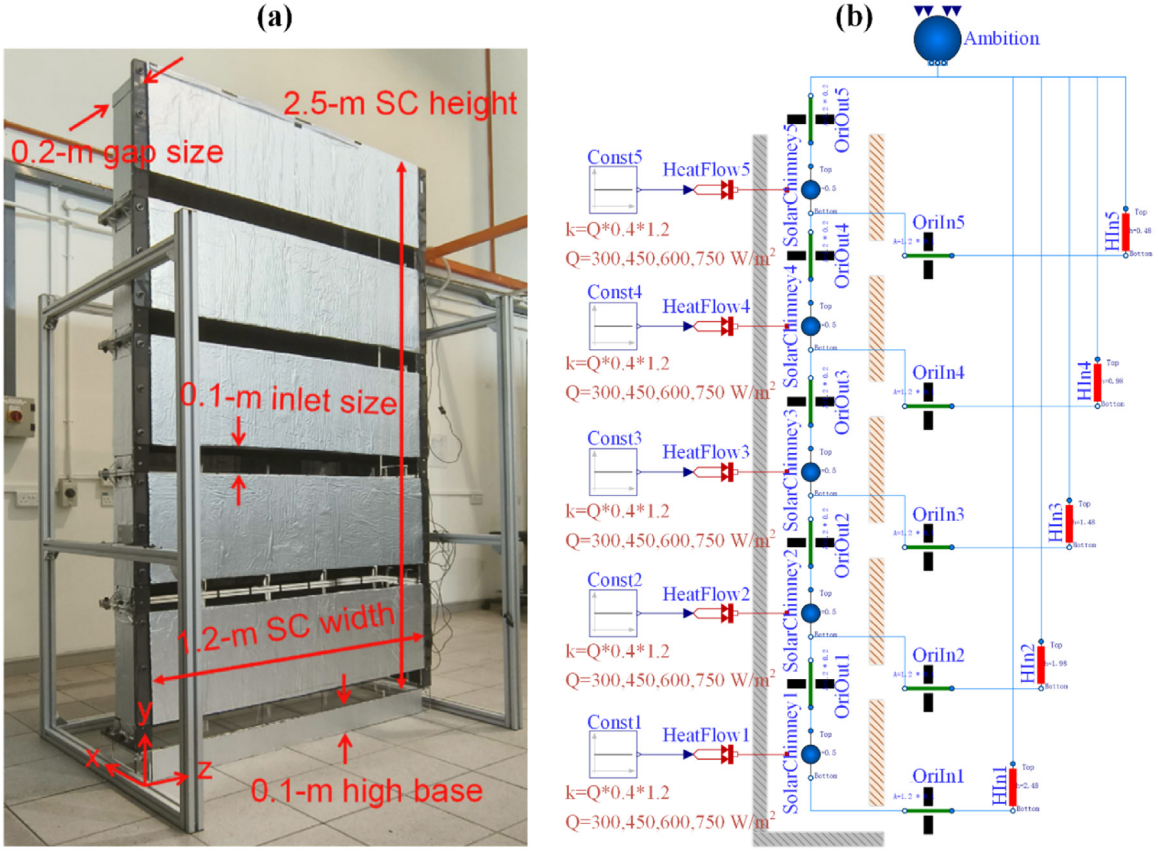


Fig. 7. Validation of the solar chimney with multiple inlets. (a) Test rig, (b) Modelica model.

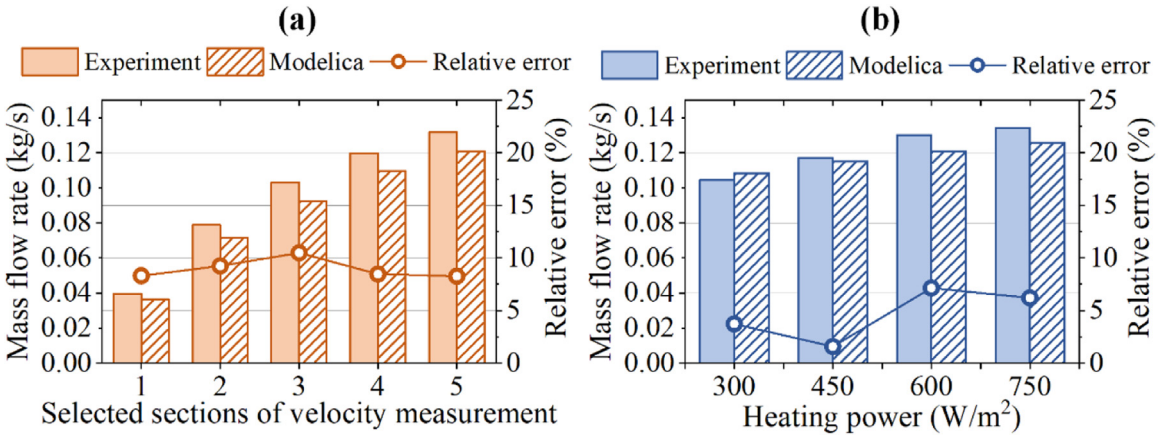


Fig. 8. Validation results. (a) At the five sections (i.e., the 1st inlet, the 2nd to the 5th outlets) under 600 W/m^2 heating power, (b) At the top outlet under various heating conditions.

story of the five-story chimney cavity test rig had identical inner dimensions of 1.2 $m \times 0.2\ m \times 0.5$ m, an air inlet of 1.2 $m \times 0.1$ m. The ambient temperature of the air-conditioned lab was at around 23 °C. Attached to the inner surface above each inlet, five silicon rubber heating mats of 1.2 $m \times 0.4$ m heated absorption wall under four heating powers (300, 450, 600, 750 W/m^2).

As shown in Fig. 8, the relative errors between the Modelica model and the experiment data are almost all below 10.00 %. The NMBE between simulated and experimental data are −8.96 % (at the five sections under 600 W/m^2 heating power) and −3.21 % (at the top outlet under various heating conditions), respectively, and the q_v(RMSE) are 9.48 % and 5.43 %. Therefore, the simulation model of solar chimney with multiple inlets developed by Modelica agrees well with the experiments

3. Results and discussion

3.1. Configuration of solar chimney

This section focuses on the natural ventilation performance of three models: a reference model without a solar chimney structure, and two solar chimney models with different configurations (the combined and separated solar chimney) in six-story buildings.

It is noteworthy that for the reference model, no solar chimney structure is installed on the south façade and the air flow rate denotes the inlet flow through the north window. Besides, the reference building does not contain the air-conditioning system. In the case of both the combined and separated solar chimneys, it is also the airflow into the chimney cavity. With only the stack effect through the window, it is difficult to establish a consistent airflow path for introducing fresh air and discharging exhaust air within the room. Consequently, the air flow rates of the reference model remain consistently low throughout the year. Specifically, the annual mean values are 0.034 m^3/s on the 1st floor, 0.025 m^3/s on the 2nd to 5th floors, 0.027 m^3/s on the 6th floor, with proportions meeting the standard (0.05 m^3/s) at 11.4 % on the 1st floor and 0 % on other floors. Therefore, the air flow rates of the reference model are far from meeting the minimum ventilation demand during working hours. Fig. 9 illustrates the hourly variation of air flow rate of the two configurations on different typical seasonal days.

In the combined solar chimney, it can be noted that increasing the vertical height of the chimney cavity leads to improved ventilation performance. As depicted in Fig. 9(a), air flow rate diminishes with increasing the floor height, and the variations between adjacent floors mostly exceed 0.1 m^3/s. The proportion meeting the standard are 88.6 % for the 1st to 4th floors, decreasing to 65.9 % and 23.3 % for the 5th and 6th floors, respectively. The cavity inlets on the 5th and 6th floors, being closer to the outlet, experience greater obstruction from the increased flow rates on lower floors due to the shorter circuit of the stack effect. Consequently, the upper floors struggle to maintain the required volume of fresh air for extended periods.

In the separated solar chimney, illustrated in Fig. 9(b), although the chimney heights on each floor are uniform, the air flow rate tends to increase with lower floors, with relatively minor variations between adjacent flow rates. This trend arises from a slightly greater pressure difference between the lower cavity outlet and a specific atmospheric level. However, the separated solar chimney has less air flow due to the single cavity height. Besides, the proportions meeting the standard are 84.1 % for the 1st and 2nd floors, rising to 88.6 % for the 3rd to 5th floors, and dropping slightly to 79.5 % for the 6th floor. Since the flow rates remain unaffected by each other, they can still achieve high rates of ventilation compliance.

In conclusion, solar chimney configurations efficiently facilitate natural indoor air ventilation. When compared with the combined solar chimney which has uneven flow distribution, the separated solar chimney demonstrates better capability in meeting the indoor minimum fresh air flow rate demand, particularly on higher floors. In addition, its ability to provide independent ventilation on each floor offers occupants a relatively safer and healthier indoor environment, particularly in the post-pandemic era.

3.2. Geometric parameters of solar chimney

Previous research indicates that solar chimneys significantly enhance indoor ventilation, a finding corroborated in Section 3.1. To achieve a balance between construction cost and solar chimney performance, it is necessary to identify the optimum geometric dimensions. Thus, this section examines two influencing factors (cavity width and length) and analyzes their impact on solar chimney performance. It should be pointed out that the separated solar chimney features uniform dimensions for its inlet, cavity cross-section, and outlet, which enhances ventilation effectiveness. Consequently, the cavity width equals the inlet height. The optimum dimensions are obtained using a benchmark case: a separated solar chimney with a cavity width of 0.3 m and a cavity length of 3 m at noon on a typical autumn meteorological day.

The cavity length refers to the horizontal length of the solar chimney attached to the south wall. It is quite certain that a longer length brings better ventilation performance due to the increased heat gain of the glazing. Fig. 10(a) illustrates the varying trends of air flow rates resulting from changes in cavity length. As the cavity length increases, the air flow rates on each floor increase nearly linearly, with significant discrepancies. This result is consistent with the conclusion obtained by Jamie et al. [43] using a parallel flow networks analysis method. The growth ratio of air flow rate diminishes on the 1st to 5th floors and

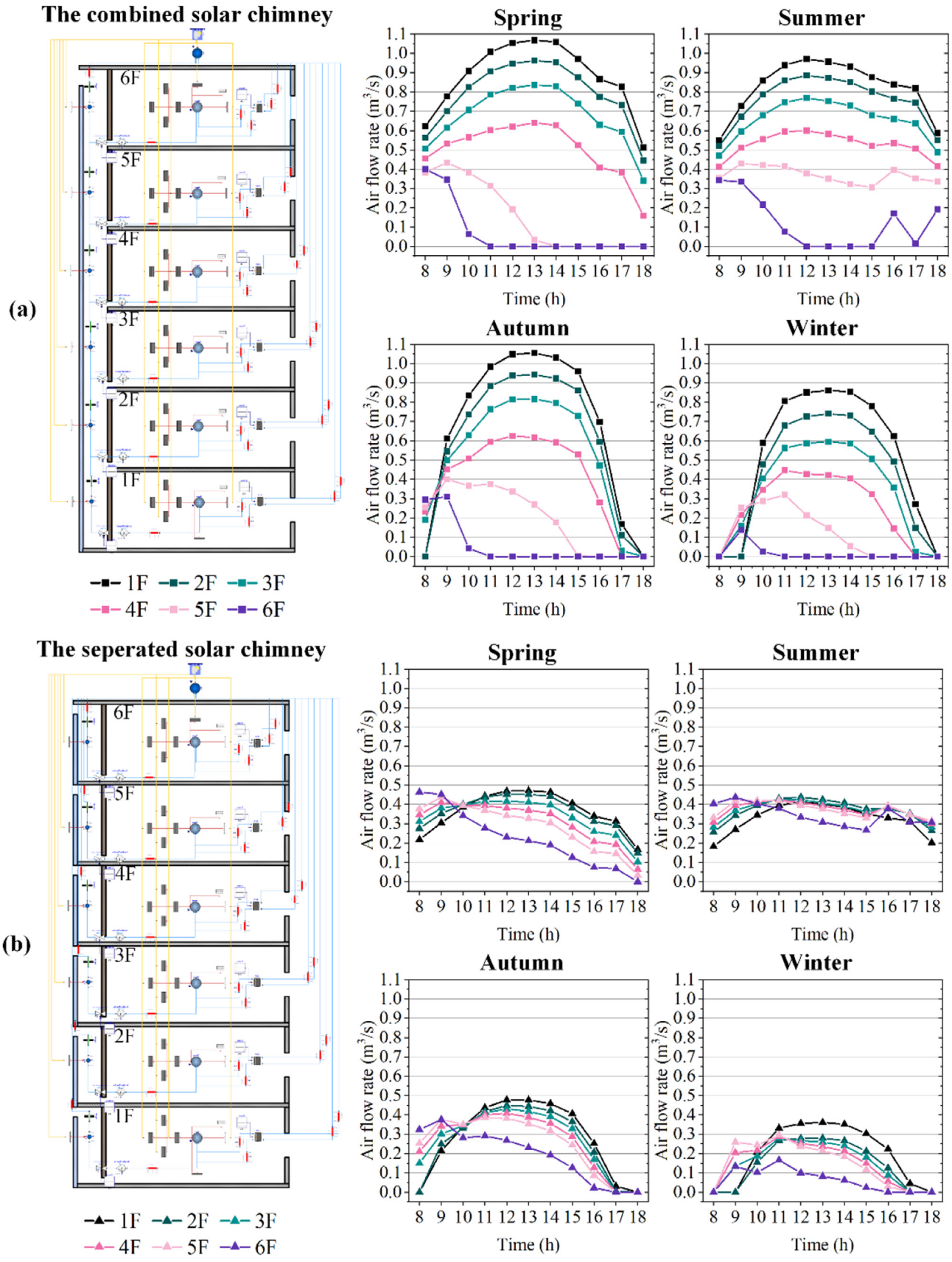


Fig. 9. Air flow rate on typical seasonal days. (a) The combined solar chimney, (b) The separated solar chimney.

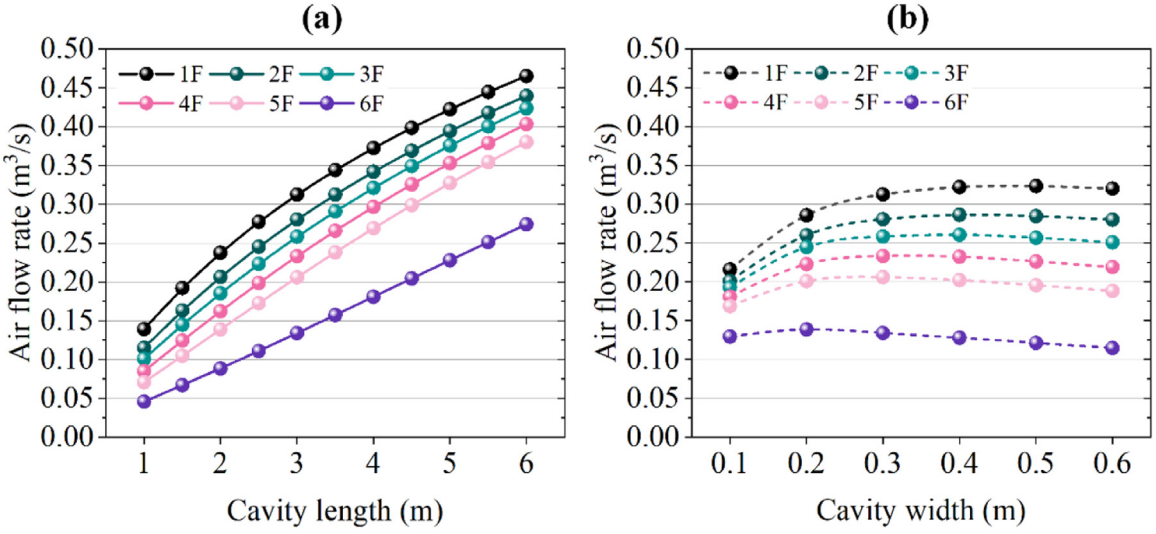


Fig. 10. Variation of air flow rate with geometric parameters. (a) Cavity length, (b) Cavity width.

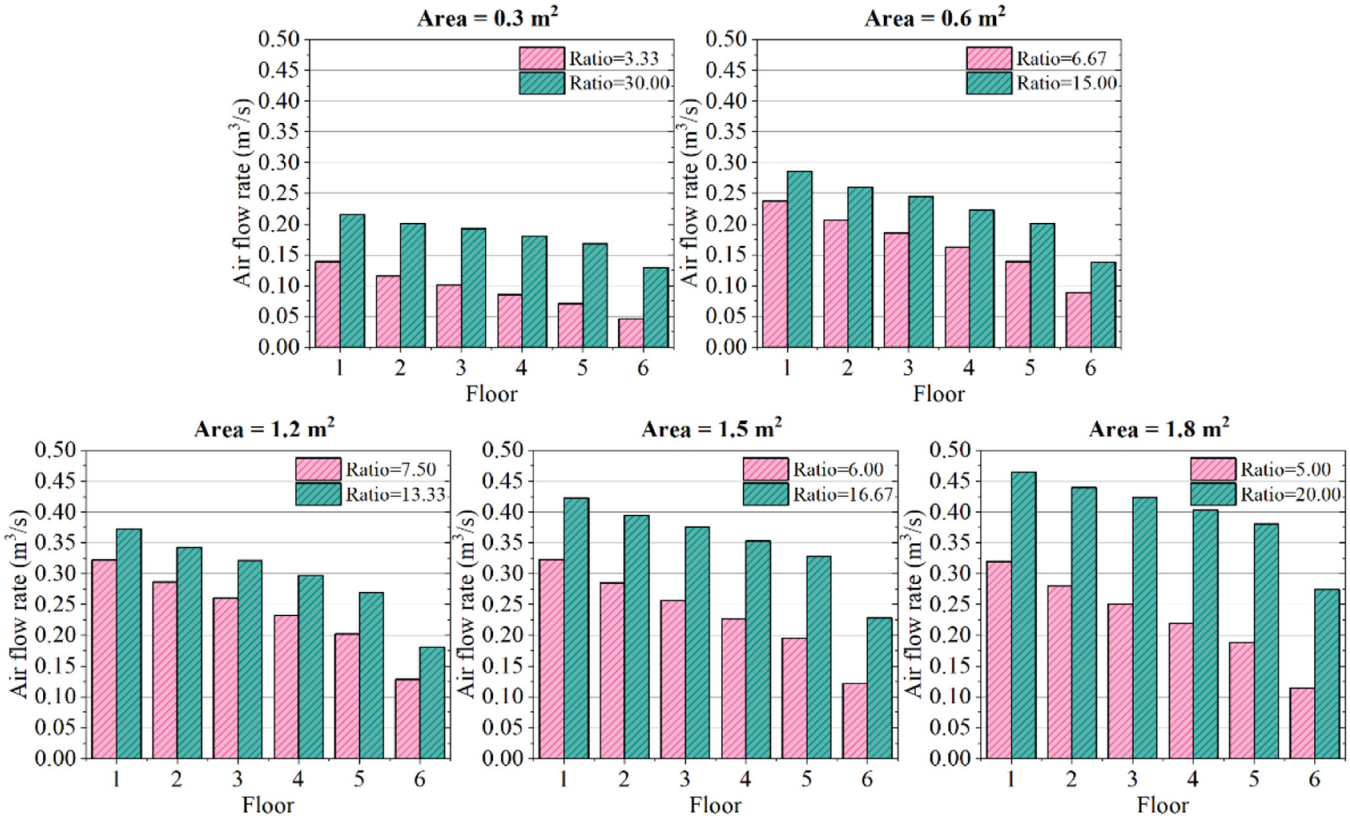


Fig. 11. Variation of air flow rate with length/width ratio.

remains relatively constant on the 6th floor. Hence, determining an optimal cavity length may not be feasible.

The cavity width, also called cavity gap or depth in some pieces of literature, refers to the distance between external glazing and the south wall. Fig. 10(b) shows the effect of the cavity width on the air flow rate predicted by the Modelica model on each floor. Within a certain range of cavity width, there is a noticeable steep increase in air flow rate, which eventually stabilizes. However, the influence of cavity width becomes insignificant or even diminishes beyond a certain value. A greater height disparity between the cavity inlet and outlet is conducive to the enhancement of the stack effect. As the inlet height (equivalent to cavity width) rises, the height disparity decreases, resulting in notable pressure losses at the inlet and outlet compared to cavity surface friction loss. Additionally, an increase in width heightens the likelihood of reverse flow due to uneven heating of air within the cavity. In summary, there exists a critical value of the cavity width at which the flow rate reaches an extreme value. These different critical values are 0.5 m for the 1st floor, 0.4 m for the 2nd and 3rd floor, 0.3 m for the 4th and 5th floor, and 0.2 m for the top floor. It also reflects that with a slightly larger pressure difference between the lower cavity outlet and a certain atmo-

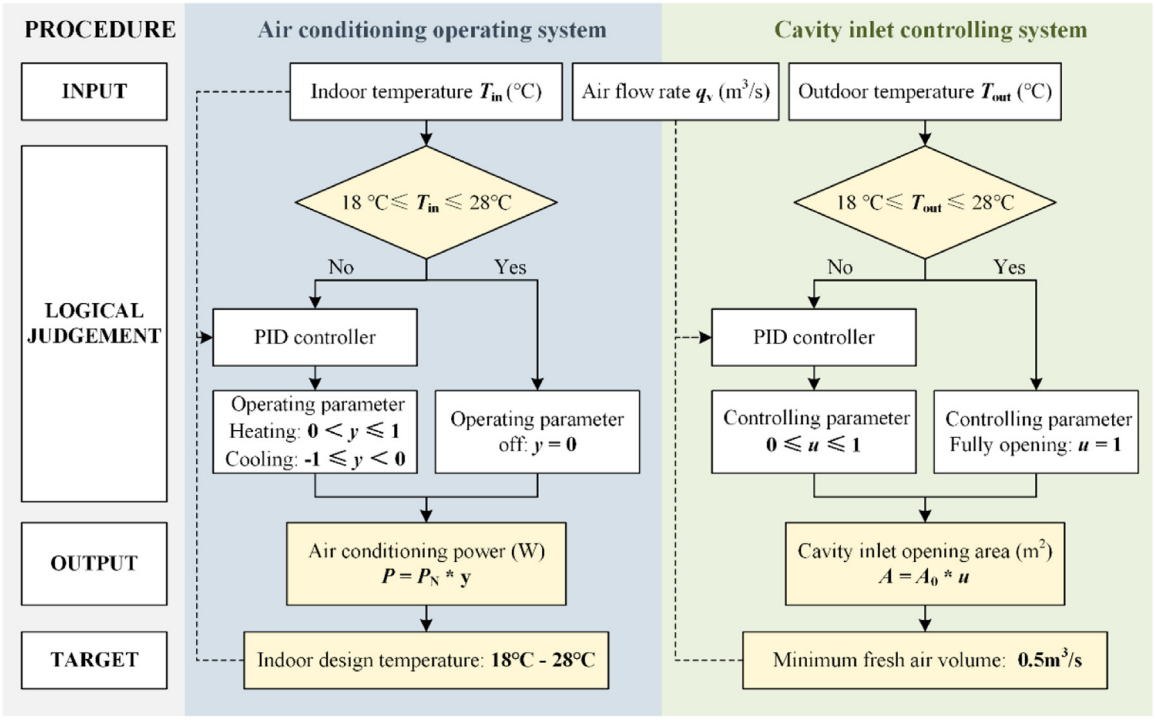


Fig. 12. Control strategy of air conditioning operating system and cavity inlet controlling system.

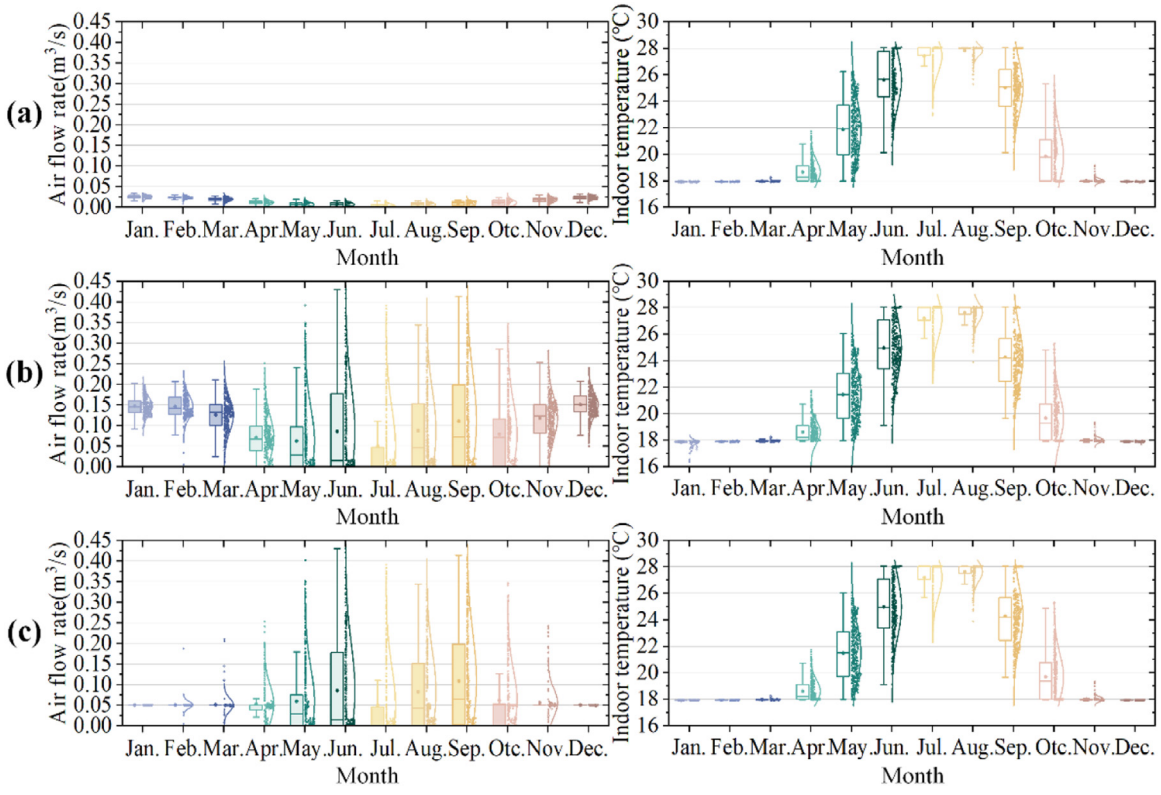


Fig. 13. Annual air flow rate and indoor temperature statistics on the 5th floor. (a) Without solar chimney, (b) Without any control, (c) With cavity inlet control.

spheric height, the effect of width becomes more remarkable. From a viewpoint of uniform design, a 0.3 m cavity width emerges as an appropriate option for this six-story building to achieve optimum ventilation effectiveness at a lower cost.

The length/width ratio refers to the ratio between cavity length and width for solar chimney and is derived from the combination of the two factors. Fig. 11 illustrates the effect of different ratios under identical cross-sectional areas of the cavity in five groups. It can be found that as the length/width ratios increase, the air flow rates rise by 108.8 %, 36.1 %, 26.8 %, 54.5 %, and 82.8 % for areas of 0.3 m^2, 0.6 m^2, 1.2 m^2, 1.5 m^2, 1.8 m^2, respectively. This phenomenon is attributed to the effect of cavity length on enhancing ventilation. In addition, for the smaller

length/width ratio, the impact of increasing the area is less evident when the area is from 1.2 m^2 to 1.8 m^2. This observation aligns with the inhibition effect of chimney width beyond the critical value.

3.3. Influence of control strategy on ventilation and energy consumption

During non-transitional seasons, excessive outdoor airflow introduced by solar chimneys is often unfavorable to indoor thermal comfort. Hence, while utilizing the air conditioning system to regulate indoor temperature, it becomes essential to control the passive ventilation rate of the solar chimney to minimize energy consumption. This section focuses on regulating the opening scale of the critical orifice (chimney cavity inlet) in the model. Building upon the analyses of Sections 3.1 and 3.2, further investigation will be conducted based on the separated solar chimney with a 3 m cavity length and 0.3 m width. Furthermore, to ensure the consistency between simulated and actual building performance, it is imperative to establish window opening behaviors that reflect realistic window operation patterns for integration. Combined with the window opening model developed for hot summer and cold winter areas obtained by Zhou et al. [44], the window opening behavior in this study is elaborated and presented in Table 3. Outdoor temperature, categorized into six intervals, is the main factor driving the window operation behavior.

As shown in Fig. 12, the Modelica model employs two primary control strategies. To maintain indoor thermal comfort throughout varying outdoor climate conditions year-round, the air conditioning system operates automatically. Its strategy relies on monitoring indoor temperature. The PID controller assesses the error parameters between the indoor temperature and the target and adjusts the operating parameter y accordingly. Subsequently, the air conditioning system modulates the output of cooling/heating power to approach the desired temperature. Additionally, to adjust ventilation performance and reduce the energy consumption of air conditioning, the area of the cavity inlet can be regulated using valves that conform to the IEC534/ISAS.75 valve size standard. These valves regulate the incompressible fluid flow through a controllable opening area. When the monitored outdoor temperature falls within the range of 18 to 28 °C, the chimney inlet valve fully opens and ventilation capacity reaches the maximum. Conversely, if the outdoor temperature deviates from this range, the PID controller evaluates the error parameters between the measured air flow rate and the target, and adjust the controlling parameter u to achieve a suitable inlet area.

To assess the effectiveness of the control strategies, three models are simulated under various ventilation conditions: one without a solar chimney, one without any control, and one with cavity inlet control. The annual ventilation rate and indoor temperature data are collected for

Table 3
Window opening behavior based on outdoor temperature.

Outdoor Temperature T_{out} (°C)	Opening status of window (%)
$T_{out} < 5$	3
$5 < T_{out} \leq 18$	5
$18 < T_{out} \leq 24$	40
$24 < T_{out} \leq 28$	60
$28 < T_{out} \leq 32$	50
$T_{out} > 32$	30

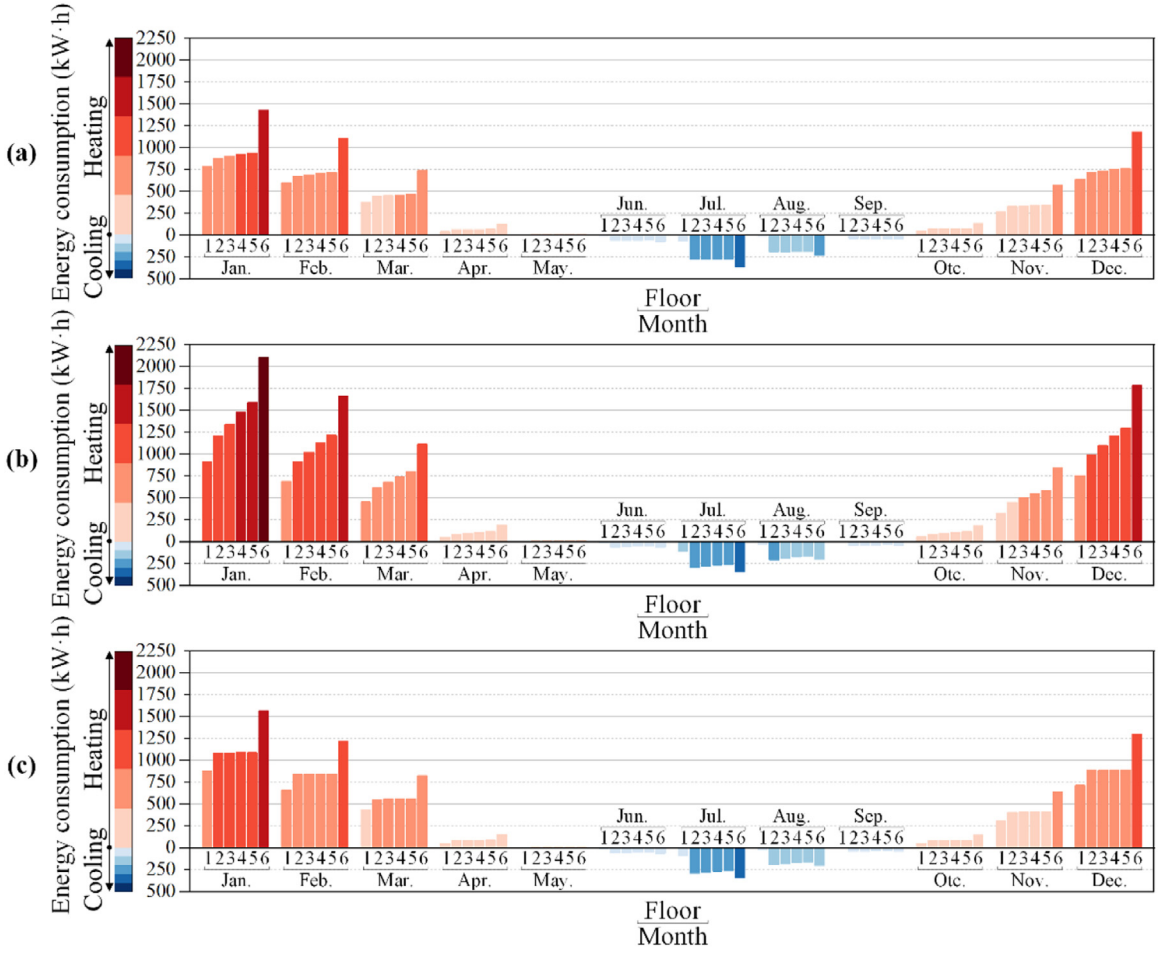


Fig. 14. Annual air conditioning energy consumption on each floor. (a) Without solar chimney, (b) Without any control, (c) With cavity inlet control.

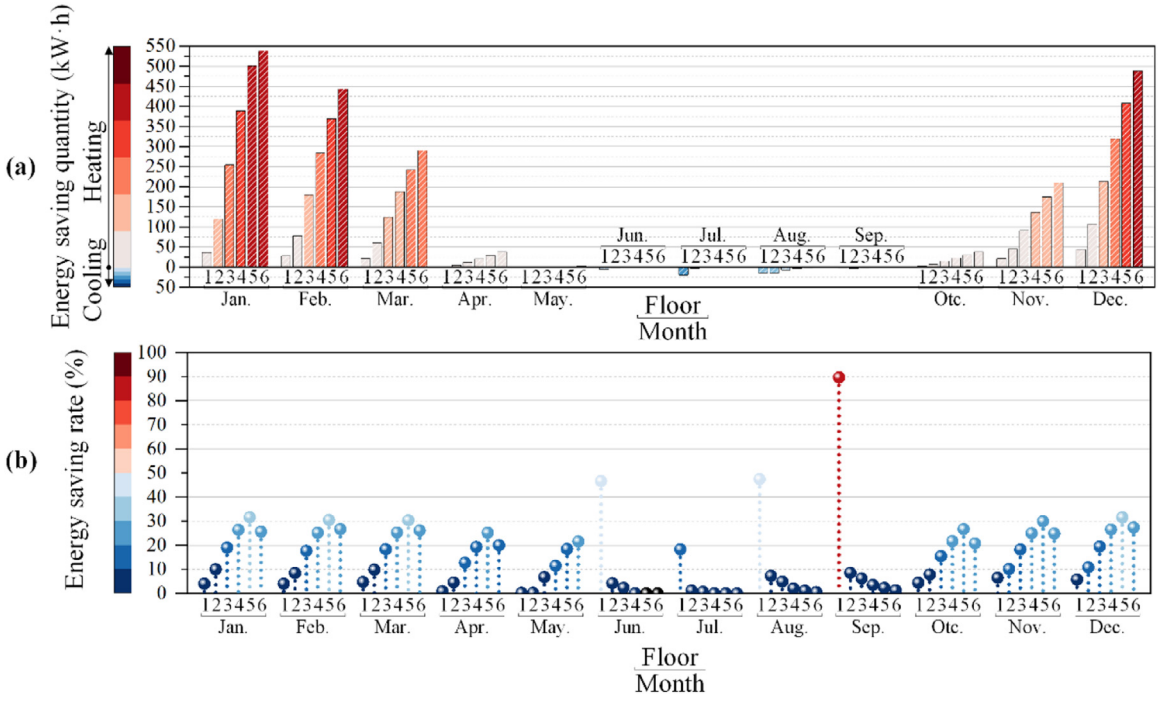


Fig. 15. Annual air conditioning energy saving on each floor. (a) Energy saving quantity, (b) Energy saving rate.

analysis. It is observed that the variation trend on each floor is similar. Therefore, the 5th Floor is chosen as a representative example, depicted in Fig. 13. In the office building without a solar chimney, although the indoor temperature remains within the designated range, the ventilation rate always fails to meet the fresh air demand. Upon the installation of a solar chimney, the annual air flow rate experiences a significant improvement. The median of the box plot indicates a greater increase during autumn and winter compared to spring and summer. This discrepancy is attributed to the larger temperature difference between indoor and outdoor environments in autumn and winter, resulting in a more pronounced influence on stack effect ventilation. However, in January, excessive ventilation leads to the inability of the air conditioning system to cope with the heating load, including the fresh air load. Therefore, the indoor temperature falls below the design threshold at some moments. Implementing a control strategy on the chimney cavity inlet ensures continuous compliance with design temperature requirements while maintaining ventilation standards. Moreover, there is a notable reduction in air conditioning energy consumption, as illustrated below.

Fig. 14(a–c) shows the annual energy consumption of the air conditioning system on each floor in the three Modelica models with different constructions. Throughout the year, during the transition seasons, when the ambient temperature occasionally exceeds 28 ˚C or falls below 18 ˚C, the air conditioning energy consumption approaches zero. Due to the increased heating load from fresh air and the enclosure structure, heating energy surpasses cooling energy. Moreover, the higher air volume generated by the solar chimney in winter further increases the heating energy. Implementing a control strategy over the flow effectively reduces heating energy consumption. From the perspective of each floor, the bottom and top floors are mainly influenced by heat transfer from the ground and the ceiling respectively, resulting in consistently minimal and maximal energy consumption. In contrast, the energy consumption of the middle floors mainly originates from the fresh air load generated by the solar chimney. Thus, their energy consumption increases in winter and decreases in summer with ascending floors.

The energy savings achieved through the cavity inlet control strategy are depicted in Fig. 15(a). The system effectively reduces the air conditioning energy consumption by 970.90 kWh, with the majority (71.5 %) of these savings occurring in winter. Additionally, energy consumption remains relatively similar in spring and autumn, accounting for 15.4 % and 11.9 %, respectively. Due to the limited volume of stack effect ventilation generated by solar radiation, energy consumption in summer is minimal, resulting in the lowest savings. In Fig. 15(b), it can be seen that during the heating season with the highest energy consumption, the energy savings range from 4 % to 30 %. Moreover, the annual saving rate of total energy consumption is calculated to be 19.6 %.

4. Conclusions

This study examines the annual ventilation and energy performance of a six-story office building equipped with a solar chimney in hot summer and cold winter areas, based on Modelica simulation. A simulation model is developed and validated to predict the air flow rate and indoor temperature of the solar chimney building with varying configurations, geometric dimension parameters, and control strategies. Several key conclusions emerged from this investigation:

(1) As for the configurations of solar chimneys, the combined solar chimney generates a higher airflow, but with uneven distribution across each floor. This imbalance is particularly notable on the upper floors, where the ventilation standard is only achieved at rates of 65.9 % and 23.3 % for the 5th and 6th floors, respectively. Conversely, the total airflow of the separated solar chimney is slightly lower than that of the combined version, yet it consistently meets the minimum fresh air requirement on each floor, ranging from 79.5 % to 88.6. Besides, the separated solar chimney facilitates the creation of independent ventilation zones for each floor, particularly beneficial during periods of infectious diseases.

(2) By studying the influence of several geometric parameters on the flow rate of the separated solar chimney, it is found that increasing cavity length leads to a continuous rise in airflow with a slightly decreasing growth ratio. Besides, as the cavity width increases, the airflow rate rises initially. However, upon reaching a critical value, the air flow rate peaks and subsequently decreases.

The critical values for cavity width are 0.5 m, 0.4 m, 0.4 m, 0.3 m, 0.3 m, and 0.2 m for the 1st to 6th floors, respectively. Moreover, with equal cavity inlet area, airflow rates increase by 108.8 %, 36.1 %, 26.8 %, 54.5 %, and 82.8 % for areas of 0.3 m^2, 0.6 m^2, 1.2 m^2, 1.5 m^2, and 1.8 m^2, respectively, as the length/width ratios increase.

(3) In winter, the temperature difference between indoor and outdoor results in excessive ventilation rate of thermal stack effect and substantial heating energy usage. The control strategy of the cavity inlet demonstrates considerable energy savings, totaling 970.9 kWh, with 71.5 % of these savings occurring during winter months. Conversely, during summer, the ventilation generated by solar radiation often fails to meet the minimum fresh air volume, particularly during cloudy weather, resulting in a lower cooling energy demand for fresh air. Consequently, mechanical fresh air systems become necessary. Overall, this control strategy yields a 19.6 % reduction in total energy consumption over a year.

Based on Modelica multizone simulations, this study evaluates the stack effect ventilation and energy consumption performance of a multi-story office building. The optimum design and control strategy obtained by this research can serve as guidance for the practical implementation of solar chimneys.

Declaration of competing interest

The authors declare that they have no known competing financial interests or personal relationships that could have appeared to influence the work reported in this paper.

CRediT authorship contribution statement

Yimin Liao: Writing – original draft, Methodology, Investigation, Conceptualization. **Zhi Gao:** Writing – review & editing, Supervision, Funding acquisition. **Fusuo Xu:** Writing – review & editing.

Acknowledgment

This work was supported by the National Natural Science Foundation of China (Grant No. 52278110).

References

[1] D. Ürge-Vorsatz, L.F. Cabeza, S. Serrano, C. Barreneche, K. Petrichenko, Heating and cooling energy trends and drivers in buildings, Renew. Sustain. Energy Rev. 41 (2015) 85–98, doi:10.1016/j.rser.2014.08.039.
[2] L. Shi, X. Cheng, L. Zhang, Z. Li, J. Tu, Interaction effect of room opening and air inlet on solar chimney performance, Appl. Therm. Eng. 159 (2019) 113877, doi:10.1016/j.applthermaleng.2019.113877.
[3] A. Bouabidi, H. Nasraoui, A. Ayadi, Z. Driss, M.S. Abid, Numerical and experimental study of the solar chimney with divergent collector, Heat Transf. Res. 9 (2019) 50, doi:10.1615/HeatTransRes.2018024769.
[4] L. Shi, A. Ziem, G. Zhang, J. Li, S. Setunge, Solar chimney for a real building considering both energy-saving and fire safety–a case study, Energy Build 221 (2020) 110016, doi:10.1016/j.enbuild.2020.110016.
[5] X.Q. Zhai, Z.P. Song, R.Z. Wang, A review for the applications of solar chimneys in buildings, Renew. Sustain. Energy Rev. 15 (2011) 3757–3767, doi:10.1016/j.rser.2011.07.013.
[6] D.S. Lee, T.C. Hung, J.R. Lin, J. Zhao, Experimental investigations on solar chimney for optimal heat collection to be utilized in organic Rankine cycle, Appl. Energy 154 (2015) 651–662, doi:10.1016/j.apenergy.2015.05.079.
[7] K.H. Lee, R.K. Strand, Enhancement of natural ventilation in buildings using a thermal chimney, Energy Build. 41 (6) (2009) 615–621, doi:10.1016/j.enbuild.2008.12.006.
[8] T. Miyazaki, A. Akisawa, T. Kashiwagi, The effects of solar chimneys on thermal load mitigation of office buildings under the Japanese climate, Renew. Energy 31 (7) (2006) 987–1010, doi:10.1016/j.renene.2005.05.003.
[9] M.M. Aboulnaga, S.N. Abdrabboh, Improving night ventilation into low-rise buildings in hot-arid climates exploring a combined wall–roof solar chimney, Renew. Energy 19 (1–2) (2000) 47–54, doi:10.1016/S0960-1481(99)00014-2.
[10] A.P. Haghighi, M. Maerefat, Solar ventilation and heating of buildings in sunny winter days using solar chimney, Sustain. Cities Soc. 10 (2014) 72–79, doi:10.1016/j.scs.2013.05.003.
[11] D. Yang, P. Li, Natural ventilation of lower-level floors assisted by the mechanical ventilation of upper-level floors via a stack, Energy Build 92 (2015) 296–305, doi:10.1016/j.enbuild.2015.01.065.
[12] Q. Wang, G. Zhang, Q. Wu, L. Shi, Ventilating aged-care center based on solar chimney: design and theoretical analysis, Energy Build 266 (2022) 122145, doi:10.1016/j.enbuild.2022.112145.
[13] K.T. Andersen, Theory for natural ventilation by thermal buoyancy in one zone with uniform temperature, Build. Environ. 38 (11) (2003) 1281–1289, doi:10.1016/S0360-1323(03)00132-X.
[14] L. Shi, G. Zhang, An empirical model to predict the performance of typical solar chimneys considering both room and cavity configurations, Build. Environ. 103 (2016) 250–261, doi:10.1016/j.buildenv.2016.04.024.
[15] E.P. Sakonidou, T.D. Karapantsios, A.I. Balouktsis, D. Chassapis, Modeling of the optimum tilt of a solar chimney for maximum air flow, Sol. Energy 82 (1) (2008) 80–94, doi:10.1016/j.solener.2007.03.001.
[16] G. He, J. Zhang, S. Hong, A new analytical model for airflow in solar chimneys based on thermal boundary layers, Sol. Energy 136 (2016) 614–621, doi:10.1016/j.solener.2016.07.041.
[17] G. He, Q. Wu, Z. Li, W. Ge, L. Cong, Ventilation performance of solar chimney in a test house: field measurement and validation of plume model, Build. Environ. 193 (3) (2021) 107648, doi:10.1016/j.buildenv.2021.107648.
[18] J. Martı´-Herrero, M.R. Heras-Celemin, Dynamic physical model for a solar chimney, Sol. Energy 81 (5) (2007) 614–622, doi:10.1016/j.solener.2006.09.003.
[19] H. Zhang, Y. Tao, G. Zhang, J. Li, S. Setunge, L. Shi, Impacts of storey number of buildings on solar chimney performance: a theoretical and numerical approach, Energy 261 (2022) 125200, doi:10.1016/j.energy.2022.125200.
[20] S. Hong, G. He, W. Ge, Q. Wu, D. Lv, Z. Li, Annual energy performance simulation of solar chimney in a cold winter and hot summer climate, Build. Simul. 12 (5) (2019) 847–856, doi:10.1007/s12273-019-0572-y.
[21] L. Moosavi, M. Zandi, M. Bidi, Experimental study on the cooling performance of solar-assisted natural ventilation in a large building in a warm and humid climate, J. Build. Eng. 19 (2018) 228–241, doi:10.1016/j.jobe.2018.04.026.
[22] W. Ding, Y. Hasemi, T. Yamada, Natural ventilation performance of a double-skin façade with a solar chimney, Energy Build. 37 (4) (2005) 411–418, doi:10.1016/j.enbuild.2004.08.002.
[23] J. Gong, K.X. Cheng, H. Liu, L.W. Chew, P.S. Lee, A novel staggered split absorber design for enhanced solar chimney performance, Build. Environ. 224 (2022) 109569, doi:10.1016/j.buildenv.2022.109569.
[24] B. Liu, X. Ma, X. Wang, C. Dang, Q. Wang, R. Bennacer, Experimental study of the chimney effect in a solar hybrid double wall, Sol. Energy 115 (2015) 1–9, doi:10.1016/j.solener.2015.02.012.
[25] S. Jafari, V. Kalantar, Numerical simulation of natural ventilation with passive cooling by diagonal solar chimneys and windcatcher and water spray system in a hot and dry climate, Energy Build 256 (2022) 111714, doi:10.1016/j.enbuild.2021.111714.
[26] S. Suhendri, M. Hu, Y. Su, J. Darkwa, S. Riffat, Performance evaluation of combined solar chimney and radiative cooling ventilation, Build. Environ. 209 (2022) 108686, doi:10.1016/j.buildenv.2021.108686.
[27] A. Sengupta, D.P. Mishra, S.K. Sarangi, Computational performance analysis of a solar chimney using surface modifications of the absorber plate, Renew. Energy 185 (2022) 1095–1109, doi:10.1016/j.renene.2021.12.089.
[28] G. Gan, Simulation of buoyancy-driven natural ventilation of buildings–impact of computational domain, Energy Build 42 (8) (2010) 1290–1300, doi:10.1016/j.enbuild.2010.02.022.
[29] J. Axley, Multizone airflow modeling in buildings: history and theory, HVAC&R Res. 13 (6) (2011) 907–928, doi:10.1080/10789669.2007.10391462.
[30] W.S. Dols, S.J. Emmerich, B.J. Polidoro, Coupling the multizone airflow and contaminant transport software CONTAM with EnergyPlus using co-simulation, Build. Simul. 9 (4) (2016) 469–479, doi:10.1007/s12273-016-0279-2.
[31] F. Xu, Z. Gao, Study on indoor air quality and fresh air energy consumption under different ventilation modes in 24-hour occupied bedrooms in Nanjing, using Modelica-based simulation, Energy Build. 257 (2022), doi:10.1016/j.enbuild.2021.111805.
[32] W. Zuo, M. Wetter, W. Tian, D. Li, M. Jin, Q. Chen, Coupling indoor airflow, HVAC, control and building envelope heat transfer in the ModelicaBuildingslibrary, J. Build. Perform. Simul. 9 (4) (2015) 366–381, doi:10.1080/19401493.2015.1062557.
[33] M. Wetter, Multizone airflow model in modelica, in: Proceedings of the Modelica 2006, 2006.
[34] L. Stephan, A. Bastide, T. Wurtz, B. Souyri, Ensuring desired natural ventilation rate by means of optimized openings, in: Eleventh International IBPSA Conference, Glasgow, Scotland, 2009, pp. 2282–2288.
[35] F. Kuznik, K. Johannes, E. Franquet, L. Zalewski, S. Gibout, P. Tittelein, J.P. Dumas, D. David, J.P. Bédécarrats, S. Lassue, Impact of the enthalpy function on the simulation of a building with phase change material wall, Energy Build. 126 (2016) 220–229, doi:10.1016/j.enbuild.2016.05.046.
[36] S. Tomažič, V. Logar, Ž. Kristl, A. Krainer, I. Škrjanc, M. Košir, Indoor-environment simulator for control design purposes, Build. Environ. 70 (2013) 60–72, doi:10.1016/j.buildenv.2013.08.026.
[37] E. Leang, P. Tittelein, L. Zalewski, S. Lassue, Numerical study of a composite Trombe solar wall integrating microencapsulated PCM, Energy Procedia 122 (2017) 1009–1014, doi:10.1016/j.egypro.2017.07.467.
[38] F. Gloriant, P. Tittelein, A. Joulin, S. Lassue, Modeling a triple-glazed supply-air window, Build. Environ. 84 (2015) 1–9, doi:10.1016/j.buildenv.2014.10.017.
[39] A. Boucher, Solar Induced Ventilation in the Algerian and Similar Climates, University of Leeds, 1989.
[40] Z. Yi, Y. Lv, D. Xu, J. Xu, R. Yang, A transparent radiative cooling film for building energy saving, Energy Built Environ. 2 (2020) 214–222, doi:10.1016/j.enbenv.2020.07.003.

[41] L. Shi, G. Zhang, An empirical model to predict the performance of typical solar chimneys considering both room and cavity configurations, Build. Environ. 103 (2016) 250–261, doi:10.1016/j.buildenv.2016.04.024.
[42] J. Gong, L.W. Chew, P. Lee, Shape optimization of high-rise solar chimneys to improve the uniformity of flowrate distribution, Build. Environ. 243 (2023) 110650, doi:10.1016/j.buildenv.2023.110650.
[43] J.P. Fine, S. Zhang, Y. Li, M.F. Touchie, Analysis of solar chimney ventilation systems in high-rise residential buildings using parallel flow networks, Build. Environ. 218 (2022) 109096, doi:10.1016/j.buildenv.2022.109096.
[44] P. Zhou, H. Wang, F. Li, Y. Dai, C. Huang, Development of window opening models for residential building in hot summer and cold winter climate zone of China, Energy Built Environ. 3 (2022) 363–372, doi:10.1016/j.enbenv.2021.03.003.